Evaluating saturation degree changes in excavation disturbed zone by stochastic differential equation

Y. Togashi [1], K. Mizuo [2], M. Osada [1], T. Yamabe [3] and H. Kameya [4]

[1]Graduate School of Science and Engineering, Saitama University
[2]Staff Service Engineering Corporation, formerly Saitama University
[3]Crown Institute
[4]OYO Corporation

Key Points:

- Exact solution of Richards equation, considering Neumann boundary, was derived to explain drying deformation phenomena.
- A new stochastic differential equation that can express water content changes in excavation disturbed zone was developed.
- Validity of the proposed exact solution and stochastic differential equation was confirmed using experimental data.

Corresponding author: Yota Togashi, togashi@mail.saitama-u.ac.jp

Abstract

In addition to changes in the deformation characteristics of rock masses based on the water content, relatively significant deformation occurs in sedimentary rocks from saturation to drying. In tunnel construction, with extremely small allowable displacements, such as geological disposal, it is necessary to properly evaluate such drying deformation phenomena. In such scenarios, it is also essential to not only evaluate the deformation characteristics, but also to assess the changes in water content in the rock mass accurately. During tunneling, excavation disturbed zone (EDZ) spreads around the tunnel due to excavation. The EDZ has a larger hydraulic conductivity than that of an intact bedrock because of which it is essential to develop a method for predicting water changes in the EDZ within the scope of the drought deformation phenomena. In this study, we derived the exact solution of the Richards equation at the Neumann boundary that could describe the desiccation phenomena in sedimentary rocks. Based on tuff samples collected in Japan, a permeability test via the flow pump method and a mercury intrusion porosimetry test were carried out to obtain the water diffusion coefficient and to verify whether the drying behavior can be described by the exact solution. Using the verified exact solution, we proposed a new stochastic differential equation that could explain the local decrease in permeability and the increase in variations in the area affected by excavation. Finally, we proposed a new method for evaluating the variation in the saturation degree distribution around a tunnel using the one-dimensional stochastic differential equation.

1 Introduction

Understanding the deformation characteristics of sedimentary rocks during tunnel construction with small allowable displacements, such as in geological disposal, is highly important. In particular, the deformation characteristics of sedimentary rocks change significantly depending on the water content. Examining the drying deformation phenomena associated with the inflow of air during tunnel excavation is of particular importance (Osada, 2014). A recent study, using tuff with deformation anisotropy, found that the principal strain orientation rotated with changes in saturation, and the relatively hard and soft directions completely reversed (Togashi, Imano, Osada, Hosoda, & Ogawa, 2021; Togashi, Imano, & Osada, 2021). Therefore, we must assess the distribution of saturation to accurately predict the deformation of rock masses in tunnels.

Changes in the water content in a porous medium including sedimentary rocks follows the Richards equation (Richards, 1931). Various analytical studies have been conducted based on the Richards equation (Farthing & Ogden, 2017) to obtain exact solutions (Fleming et al., 1984; Ross & Parlange, 1994). Recently, studies have proposed exact solutions incorporating various nonlinear functions, such as the water diffusion coefficient, D (Hooshyar & Wang, 2016; Broadbridge et al., 2017). Although boundary conditions such as Dirichlet boundary conditions are often used to obtain the exact solution, Neumann boundary conditions are rarely used (e.g., Barry et al., 1993). During the drying deformation phenomena, the changes in the water content of rock mass in contact with the atmosphere does not occur suddenly; hence, it is vital to define a Neumann boundary.

During tunnel excavation, the surrounding rock mass becomes loose, and the excavation disturbed zone (EDZ) expands. Hence, it is crucial to evaluate the EDZ while examining the drying deformation phenomena. Previous studies have shown that the closer to the well wall, the higher the permeability of the EDZ. (Hou, 2003; Marschall et al., 2006; Lisjak et al., 2016). Some studies have compared and modelled the water diffusion coefficients of the EDZ and normal rock (Autio et al., 1998).

Similarly, several studies have analyzed the permeability of the EDZ, but there is no unified view because its properties differ depending on location, such as the geological conditions and surface stress fields. In particular, the obtained permeability varies widely because the excavation disturbance is significant adjacent to the tunnel wall (Kurikami et al., 2008).

Therefore, in this study, we derived the exact solution of the Richards equation using the Neumann boundary, which can describe the drying phenomena in sedimentary rocks. Based on tuff samples collected in Japan, a hydraulic conductivity test and mercury intrusion test via the flow pump method were performed to obtain the water diffusion coefficients and verify whether the drying behavior can be described by the exact solution. Using the verified exact solution, we proposed a new stochastic differential equation that can express the local variations in permeability and the increases in the variation in areas affected by excavation. We proposed a new method for evaluating variations in the saturation distribution in tunnels using the proposed one-dimensional stochastic differential equation.

2 Numerical method to determine saturation degree distribution in EDZ due to drying

2.1 Exact solution of Richards equation considering Neumann boundary conditions for drying phenomena

The following nonlinear partial differential equation was proposed to predict changes in the water content in unsaturated ground (Richards, 1931):

$$\frac{\partial \theta}{\partial t} = \frac{\partial K}{\partial r}\left(\frac{\partial \psi}{\partial r} + 1\right). \tag{1}$$

where θ is the volumetric water content, t is time, K is the unsaturated hydraulic conductivity, r is the coordinate, and ψ is the pressure head. The exact solution of this nonlinear partial differential equation is not known; however, in this study, we obtained the exact solution of this equation using a method similar to that in a previous study (Barry et al., 1993). As this method was considerably simplified, the derivation is described in detail below. The Richards equation was transformed into the following:

$$\frac{\partial \theta}{\partial t} = \frac{\partial}{\partial r}\left(K\frac{\partial \psi}{\partial \theta}\frac{\partial \theta}{\partial r}\right) + \frac{\partial K}{\partial r}. \tag{2}$$

where the heat equation can be obtained by considering that the water diffusion coefficient, D, which is the slope of the water retention curve, is always a constant ($D = K\partial\psi/(\partial\theta) = \text{const.}$) (Gardner, 1958). Furthermore, we also considered that the unsaturated hydraulic conductivity does not depend on the coordinates ($\partial K/(\partial r) = 0$).

$$\frac{\partial \theta}{\partial t} = D\frac{\partial^2 \theta}{\partial r^2}. \tag{3}$$

The water retention curve is predominantly non-linear in the region adjacent to saturation and dryness. However, the assumption that D is constant in the region where S is neither too small nor too large holds. It is also rational to assume that K does not depend on coordinates if the stratum is uniform. The following can be obtained by substituting the effective saturation $S = (\theta - \theta_r)/(\theta_s - \theta_r)$ into the above equation using the volume moisture content, θ_s, at saturation and the residual volume moisture content, θ_r (Tracy, 2011):

$$\frac{\partial S}{\partial t} = D\frac{\partial^2 S}{\partial r^2}. \tag{4}$$

Further, we set the initial and boundary conditions. First, the following equation was assumed as the initial condition:

$$S(r,0) = S_i. \tag{5}$$

We considered a closed interval where r is $[0, L]$ and S_i is a constant value. Here, the following Neumann boundary conditions were introduced to manage the various boundary conditions (Farlow, 1993):

$$\frac{\partial S(0,t)}{\partial r} = 0, \quad -\frac{\partial S(\pm L,t)}{\partial r} = h(S - S_t). \tag{6}$$

where S_t is the constant terminal saturation value. Although 0 to L for the interval of r was used in this study, the exact solution was derived from $-L$ to L to obtain the necessary and sufficient boundary conditions; the result is shown by $0 \leq r \leq L$. As the exact solution cannot be obtained as it is, we introduced the dimensionless saturation degree, $s_d(r,t) = (S(r,t) - S_t)/(S_i - S_t)$, and modified the equation as follows:

$$\frac{\partial s_d}{\partial t} = D\frac{\partial^2 s_d}{\partial r^2}, \tag{7}$$

$$s_d(r,0) = \frac{S(r,t) - S_t}{S_i - S_t} = 1 \tag{8}$$

and

$$\frac{\partial s_d(0,t)}{\partial r} = 0, \quad -\frac{\partial s_d(\pm L,t)}{\partial r} = hs_d. \tag{9}$$

First, the general solution of Eq. (7) can be expressed as follows:

$$s_d = (A\cos pr + B\sin pr)\, Ce^{-Dp^2t} \tag{10}$$

where A, B, and C are undetermined coefficients and p is a non-zero positive real number. By differentiating this equation with r and substituting $r = 0$, the following was obtained from the boundary conditions in Eq. 9:

$$(-Ap\sin pr + Bp\cos pr)\, Ce^{-Dp^2t}\,|_{r=0} = BpCe^{-Dp^2t} = 0 \tag{11}$$

When C is zero, s_d is always zero; thus, $B = 0$. Similarly, by substituting the boundary condition of $r = L$ in Eq. 9, the following was obtained:

$$-(-Ap\sin pr)\, Ce^{-Dp^2t}\,|_{r=L} = Ap(\sin pL)Ce^{-Dp^2t} = hA(\cos pL)Ce^{-Dp^2t} \tag{12}$$

Therefore, the following relational expression for p was obtained:

$$p\tan pL = h \tag{13}$$

If the solutions that satisfy Eqs. (13) are $p_1,\ p_2,\ p_3\cdots$, then their linear sum is also the solution; hence s_d can be expressed as follows:

$$s_d = \sum_{n=1}^{\infty} (C_n \cos p_n r)\, e^{-Dp_n^2 t}. \tag{14}$$

Substituting the initial condition in Eq. (8) into this equation yielded the following:

$$s_d(r,0) = 1 = \sum_{n=1}^{\infty} (C_n \cos p_n r) \tag{15}$$

To determine the Fourier coefficient, C_n, the right-hand side of the above equation for n and $\cos p_m,\ (m = 1, 2, \cdots)$ were multiplied and integrated. This integral has a value only when $m = n$ owing to the orthogonality of the trigonometric function, as shown below:

$$\int_0^L C_n \cos p_n r \cdot \cos p_m r dz = C_n \left(\frac{\sin(2p_n L)}{4p_n} + \frac{L}{2} \right) \tag{16}$$

Therefore, this equation is equal to the following equation:

$$\int_0^L 1 \cdot \cos p_m r dz = \frac{\sin(p_m L)}{p_m} \tag{17}$$

From the above, C_n can be obtained as follows:

$$C_n = \frac{4\sin(p_n L)}{\sin(2p_n L) + 2p_n L} \tag{18}$$

Therefore, the exact solution of s_d is given as follows:

$$s_d = \sum_{n=1}^{\infty} \frac{4\sin(p_n L)}{\sin(2p_n L) + 2p_n L} (\cos p_n r) e^{-D p_n^2 t} \tag{19}$$

When the change in the variables in Eq. (8) is taken back, an exact solution for the saturation degree, S, can be obtained by setting $\beta_n = p_n L$.

$$S(r,t) = S_t + (S_i - S_t) \sum_{n=1}^{\infty} \frac{4\sin(\beta_n)}{\sin(2\beta_n) + 2\beta_n} (\cos \beta_n r/L) e^{-D\beta_n^2 t/L^2} \tag{20}$$

From Eq. 13, β_n is the solution to the following transcendental function, which was solved via the Newton-Raphson method:

$$\frac{\beta_n}{Lh} = \cot \beta_n \tag{21}$$

2.2 Stochastic differential equation for description of saturation degree distribution in EDZ due to drying

Unpredictable random behavior is known as Brownian motion, named after Dr. R. Brown, who discovered that pollen particles floating on the surface of the water behave irregularly. The total derivative first-order differential equation, including Brownian motion, is referred to as a stochastic differential equation in the field of financial engineering, which is used to predict and set stock prices for financial products. As ordinary Brownian motion describes future uncertainty, it is a random motion that accumulates one variance of time per unit of time.

In a homogeneous stratum, the nature of the EDZ is such that the vicinity of the excavated tunnel wall gets disturbed and develops cracks, thus resulting in heterogeneous and random properties. However, areas farther from the tunnel wall have more homogeneous properties. This can be explained by the Brownian motion of the variable r because the larger the value of r (Fig. 1), the more the variance accumulates and shows random properties. In this study, we proposed a stochastic differential equation that estimates the saturation distribution of the EDZ using the following characteristics:

$$dS^*(r,t) = dS(r,t) \left(1 + \sigma dW(r)\right). \tag{22}$$

where S^* is the saturation distribution based on the properties of the EDZ, S is the exact solution to Eq. (20), σ is the volatility that controls the magnitude of Brownian motion, and W is the Wiener process indicating Brownian motion. As the infinitesimal increment in the exact solution (Eq. (20)) is the coefficient of the term including Brownian motion, S^* always converges to S_t by $t \to \infty$, regardless of the

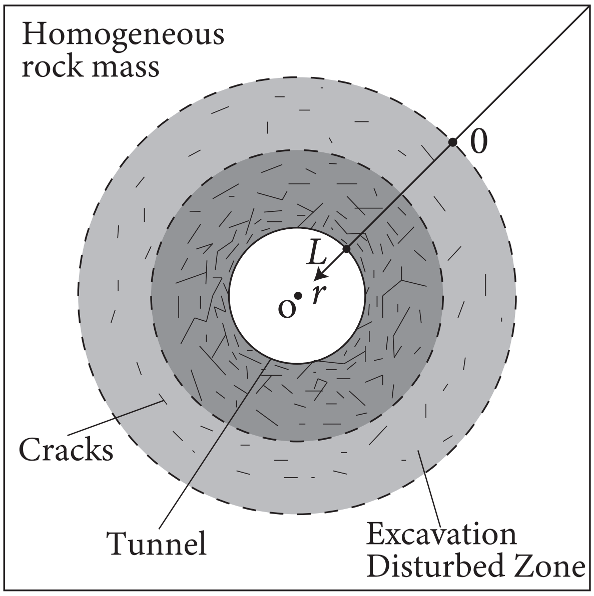

Figure 1. Concept of Excavation Disturbed Zone (EDZ). r is the coordinates toward the center of the tunnel, and L is the width of EDZ. Random characteristics become large as the coordinate r increase.

magnitude of σ. Figure 2 shows an example of Brownian motion, W, generated under this condition. Thus, the random property increases with an increase in the variable (i.e., r). So far, there have been studies discussing the increase in permeability variation in EDZ (Kurikami et al., 2008), but there is no case in which the properties of EDZ are expressed by Brownian motion.

3 Detection of hydraulic conductivity and water retention characteristics

The moisture diffusion coefficient, D, was assumed to be constant in this study. $S = (\theta - \theta_r)/(\theta_s - \theta_r)$, if θ is differentiated by S, then $\frac{dS}{d\theta} = \frac{1}{\theta_s - \theta_r}$ can be obtained. Therefore, the expansion of the formula for D is as follows:

$$\begin{aligned} D = K\frac{\partial \psi}{\partial \theta} &= K\frac{\partial \psi}{\partial S}\frac{\partial S}{\partial \theta} \\ &= K \cdot \frac{\partial \psi}{\partial S} \cdot \frac{1}{\theta_s - \theta_r}. \end{aligned} \tag{23}$$

where K is the unsaturated hydraulic conductivity. If the saturated hydraulic conductivity, k_s, is proportional to the degree of saturation, unsaturated hydraulic conductivity can be described as $K = k_s S$. Therefore, it is sufficient to determine K using the results of the saturated hydraulic conductivity test. In the above equation, θ_s and θ_r were determined using a mercury intrusion porosimetry test as the void volume in the sample can be determined by this test. $\frac{\partial \psi}{\partial S}$ is the slope of the water retention curve, which can be obtained by performing a mercury intrusion porosimetry test for rocks. The following sections detail the three tests conducted in this study to obtain D.

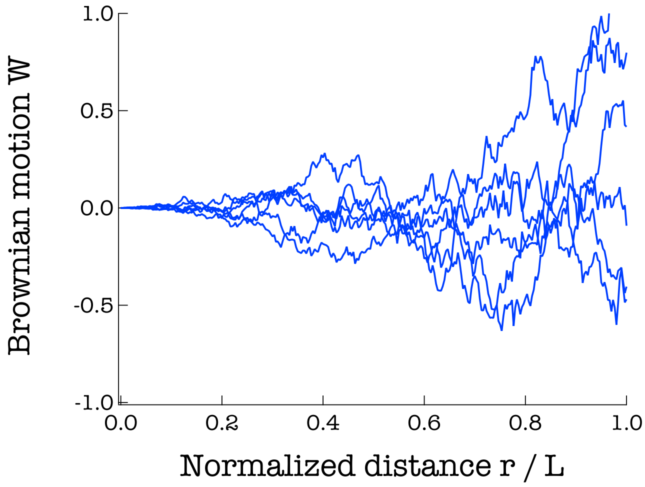

Figure 2. Relationship between random EDZ characteristics by Brownian motion and distance r. It can be expressed that the closer r is to L, the more random the property is, as shown in Fig. 1.

3.1 Rock sample

A Neogene tuff collected from a depth of 100 m in Utsunomiya City, Japan was used as the rock test sample. This marine-origin tuff was formed by the consolidation of eruptive deposits that originated from submarine volcanoes dated to 10 Mya. This green colored tuff is known as a Tage tuff, as shown in Fig. 3; it is widely used in Japan as a research sample and building material (e.g., the Old Imperial Hotel Japan designed by Frank Lloyd Wright). This tuff has uniform and homogeneous properties. The minerals contained in the Tage tuff are tuffy glass, plagio-

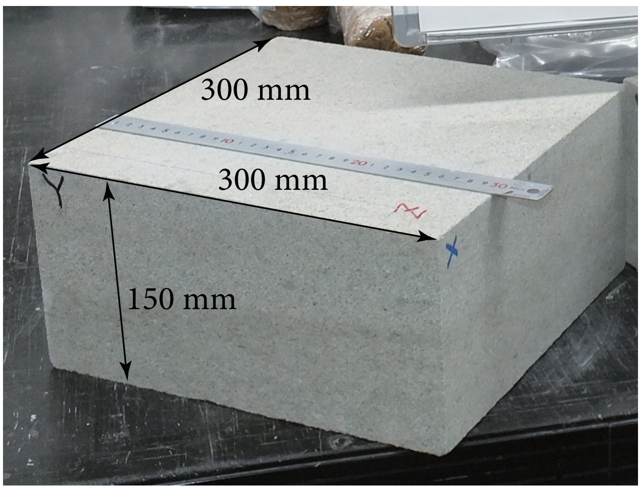

Figure 3. Cuboidal block sample of Tage tuff.

clase, quartz, and biotite amphibole pyroxene. (Seiki, 2017). Table 1 lists the physical properties of the Tage tuff. Tage tuff is characterized by a large porosity and a

Table 1. Physical properties of the Tage tuff

Density in natural state $\rho_t(\mathrm{Mg/m^3})$	Dry density $\rho_d(\mathrm{Mg/m^3})$	Wet density $\rho_t(\mathrm{Mg/m^3})$	Porosity %	Natural moisture content ratio w (%)
1.81	1.76	2.04	26.7	3.8

slightly soft deformation property (Togashi et al., 2018, 2019; Togashi, Kikumoto, et al., 2021). The porosity of the sample was determined by the soil particle density test, which yielded a density of 2.56 Mg/m^3.

3.2 Permeability test

The hydraulic conductivity was obtained using the flow pump method (Esaki et al., 1996). In this method, the saturated hydraulic conductivity was obtained by controlling the flow rate with a syringe pump, as shown in Fig. 4, and measuring the pressure head difference. Saturated hydraulic conductivity can be expressed as follows:

$$k_s = \frac{Q}{At}\frac{H}{\psi} \tag{24}$$

where Q is the controlled flow rate, A is the cross-sectional area of the specimen, t is time, and H is the length of the specimen. During this experiment, the room temperature was maintained at 22 °C while the test was conducted.

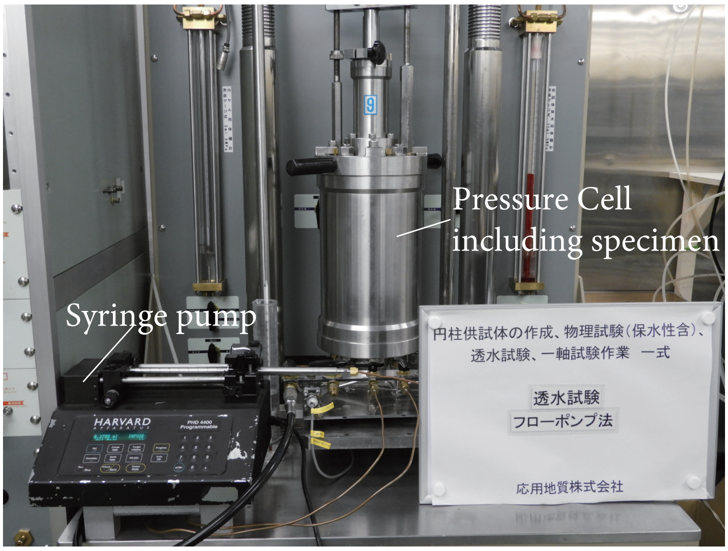

Figure 4. Permeability test based on the flow pump method

3.3 Mercury intrusion porosimetry test

In the mercury intrusion porosimetry test, mercury is press-fitted while pressurizing a dry sample, and the distribution of the gap diameter in the sample is inferred based on the pressure and the amount of press-fitted mercury (Thomas et al., 1968; ASTM, 2004). This test determines the void diameter distribution of a sample; however, in this study, it was used to determine the water retention curve as proposed in previous studies (Sun & Cui, 2020). Based on the results of this test, the saturation degree, S, was calculated as follows:

$$S = \frac{CI(P)}{CI(P_{max})} \tag{25}$$

where CI is the amount of press-fitted mercury, P is the arbitrary press-fitting pressure, and P_{max} is the maximum pressure. By investigating S using P as the capillary pressure, a water retention curve could be obtained.

3.4 Detection of continuous moisture content variation by drying deformation test

Figure 5 shows the drying deformation experiment (Togashi, Imano, Osada, Hosoda, & Ogawa, 2021). In this experiment, a strain gauge was installed on a wet rock specimen, which was air-dried. The change in the water content was measured using an electronic balance. We estimated the change in saturation by considering the change in the void structure estimated from the deformation of the specimen. The cylindrical Tage tuff specimen, with a diameter of 50 mm and height of 100 mm, had a volumetric strain of approximately 2,000 μ, with changes in its void diameter. The degree of saturation was estimated while considering the change in void diameter due to drying (Togashi, Imano, Osada, Hosoda, & Ogawa, 2021). Using the time-series changes in the saturation of the Tage tuff measured using this method, the validity of the exact solution to the Richards equation, as derived above, was verified.

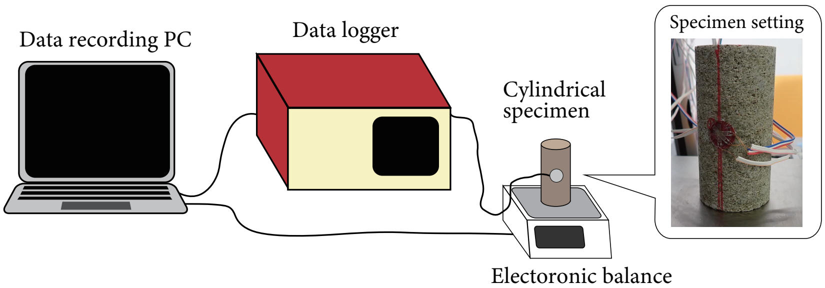

Figure 5. Drying deformation experiment (Togashi, Imano, Osada, Hosoda, & Ogawa, 2021).

4 Verification of the exact Richards equation solution

4.1 Identifying parameters that compose *D*

Table 2 lists the test results obtained in the permeability test and the mercury intrusion porosimetry tests. The saturated permeability coefficient, k_s, obtained was the average value from nine specimens. However, the permeability coefficient was rather small for its correspondingly large porosity. Similar findings have also been reported in previous studies (Watanabe & Sato, 1979); hence, the value obtained for the hydraulic conductivity was considered to be appropriate. The void volume could be obtained from the volume of the press-fitted mercury in the mercury intrusion porosimetry test. The void volume obtained was the average value of three mercury intrusion tests. Volume moisture content can be defined as θ and $\theta = \frac{V_w}{V}$, where V_w

and V are the water volume and total volume, respectively. As the volume of the void is equal to the water volume ,V_w, at saturation, the total volume, V, was calculated using the mass and dry density, ρ_s, of the sample in the mercury intrusion test; finally, the saturated volume moisture content was determined. Thus, the value of $\frac{1}{\theta_s - \theta_r}$ was 3.8, assuming $\theta_r = 0$.

Table 2. Results of the permeability test and the mercury intrusion porosimetry test

Saturated hydraulic conductivity k_s (m/s)	Void Volume (cm^3/g)	Saturated volume moisture content Moisture content θ_s
5.7×10^{-11}	0.15	0.26

Figure 6 shows the water retention curve specified by Eq. (25) in the mercury intrusion test. A value of $P = 5$ MPa, equivalent to the suction specified at $S = 0.13$, was confirmed in the dry deformation experiment of a previous study (?, ?), thus validating this result. Based on Fig. 6, the inclination of the curve was relatively constant from $S = 0.2 - -0.9$. Therefore, the value of $\frac{\partial \psi}{\partial S}$ corresponds to 341.4 m, as the suction is converted to a pressure head of $\psi = P/(\rho_w g)$, where ρ_w (= $1.0(\mathrm{g/cm^3})$) and g (= $9.81\mathrm{m/s^2}$) are the water density and gravitational acceleration, respectively. The unsaturated hydraulic conductivity, $K = Sk_s = 0.55 \times 5.7 \times 10^{-11} =$

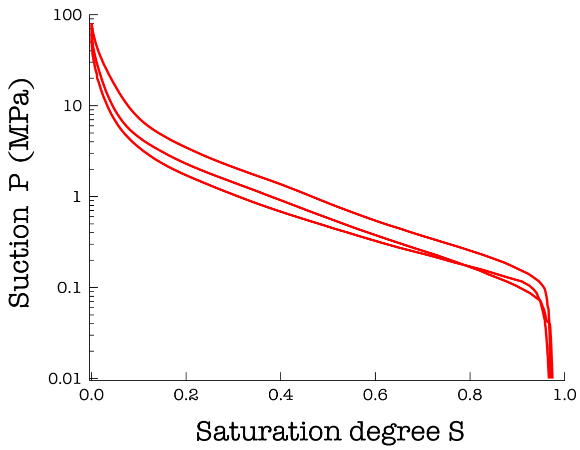

Figure 6. Water retention curve (relationship between suction P and saturation degree S) for the Tage tuff.

3.1×10^{-11} when calculated in the middle of $S = 90\% - 20\%$. Therefore, the desired D can be calculated as $D = K \cdot \frac{\partial \psi}{\partial S} \cdot \frac{1}{\theta_s - \theta_r} = 3.1 \times 10^{-11} \cdot 341.4 \cdot 3.8 = 4.02 \times 10^{-8}$ ($\mathrm{m^2/s}$). As the drying process of $S = 0.9$ to 0.2 was calculated, $\frac{\partial \psi}{\partial S}$ was set as positive in the direction of increasing suction, which is opposite to that illustrated in Fig. 6.

4.2 Nature of exact solution

Using the value of D specified in the previous section, the nature of the exact solution was assessed (Eq.20). Figure 7 shows the effect that the difference in h has on the exact solution. Table 3 lists the input parameters of the exact solution. Here, $L = 0.1$ m was set to accelerate the convergence of the saturation degree, and

Table 3. Input parameters of the exact solution.

Initial saturation degree S_i	Terminal saturation degree S_t	D (m^2/s)	L (m)	Number of Fourier series terms n
0.9	0	4.02 $\times 10^{-8}$	0.1	100

S_i and S_t were set to 0.9 and 0, respectively. To observe the nature of the solution over a wide area, we performed calculations in which $Srangedfrom0.2 - -0.9$, which assumed linearity based on the previous section. The results are shown as the distribution of the daily r for 20 d. The number of terms, n, in the Fourier series in the exact solution was set to 100. Larger h values yielded a faster convergence of the saturation degree, as well as the closer it is to the Dirichlet boundary condition. Additionally, the smaller the value of h, the closer the saturation is to a constant inside the region. By introducing the Neumann boundary condition, we could express various situations.

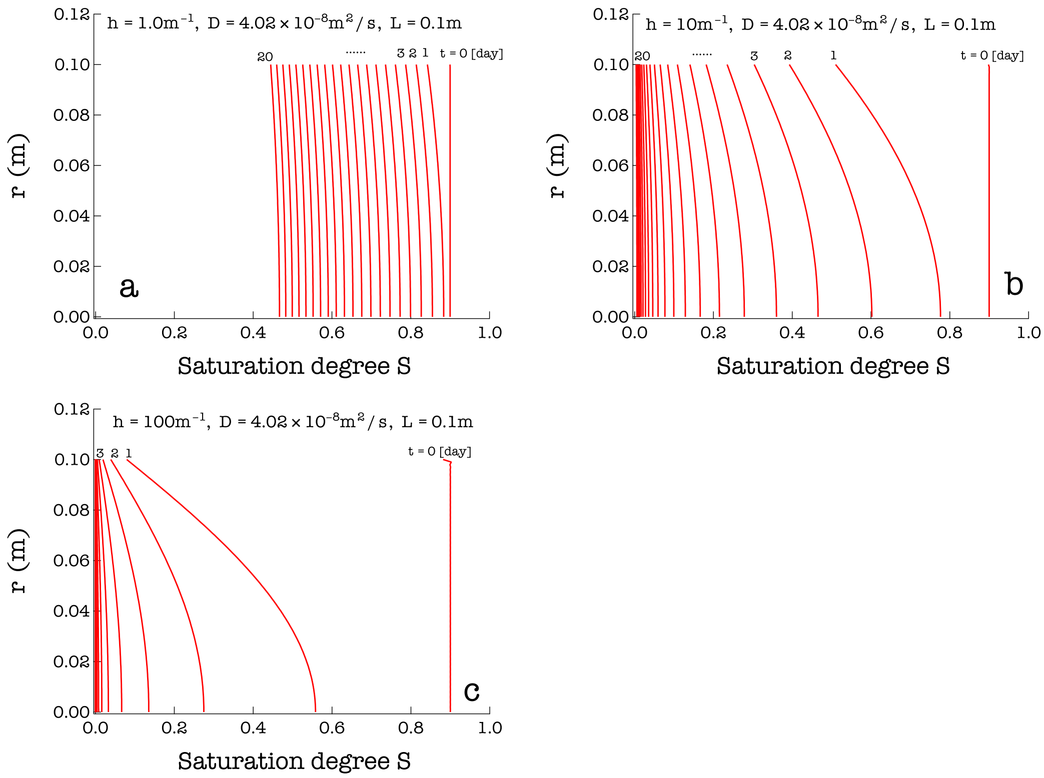

Figure 7. Characteristics of the exact solution (saturation degree S and distance r relationships) based on $D = 4.02 \times 10^{-8}$ (m^2/s): (a) $h = 1$ m^{-1}, (b) $h = 10$ m^{-1}, and (c) $h = 100$ m^{-1}.

4.3 Comparison between the exact solution and test results for verification

Figure 8 compares the proposed exact solution with the results of the dry deformation experiment. In the experimental results, the cylindrical specimen was soaked in water for $\geq$ 10 d to increase the saturation degree to approximately 0.8, and followed by air drying. Table 4 lists the input parameters of the exact solution. Here, the exact solution was calculated using the D obtained in section 4.1.S_i and S_t

Table 4. Input parameters of the exact solution.

Initial saturation degree S_i	Terminal saturation degree S_t	D (m^2/s)	h (m^{-1})	L (m)	Number of Fourier Series terms n
0.81	0	4.02×10^{-8}	12.2	0.0375	100

were set to 0.9 and 0, respectively. The exact solution exceeded the linearity range of the water retention curve assumed in the range of $S = 0.2 - -0.9$ when D was calculated in the previous section; however, we verified the error. The exact solution data showed a change in the saturation at $x = 0$, where h was set to 12.2 m^{-1}. In the experiment, the length of the region was $L = 0.0375$m, the average value of the half diameter was 25 mm, and half height was 50 mm for the cylindrical specimen. Here, L was set by assuming an element test to examine uniform behavior; however, if L was on the same level, it could be adjusted by changing h. The results were in good agreement, even in the region where S was small. As the experimental value and exact solution were nearly identical, we confirmed the validity of the proposed exact solution.

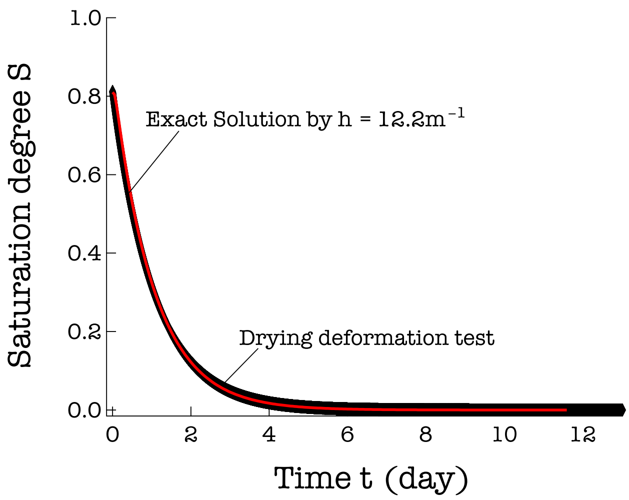

Figure 8. Comparison of saturation degree S and time t relationships between the exact solution and drying deformation test results

What we have verified here is the phenomenon of small specimen size. However, even if the width of the region L is large, the convergence of the exact solution can be delayed by reducing h as shown in Fig. 7. Therefore, if the stratum has homogeneous properties, the exact solution shown here can be applied even if the area L is large. Based on this, the proposed stochastic differential equation was discussed in the next chapter.

5 Random saturation degree distribution in the EDZ

In this section, we discuss the properties of the stochastic differential equation proposed in Eq. (22) using the exact solution, whose validity was confirmed via the drying deformation test results. Equation (22) was solved using the Eular-Maruyama method (Higham, 2001). This is a type of backward finite differential method, which can be derived as follows. For the region of $[0, L]$, let $\Delta r = r/N$ be an infinitesimal increment in the coordinate direction r. Here, N is the number of divisions in the area. Using the positive integer j, r_j can be written as $r_j = j\Delta r$. Thus, Eq. (22) can therefore be modified as follows:

$$\begin{aligned} dS^* &= dS\left(1+\sigma dW\right) \\ &= \frac{\partial S}{\partial r} dr\left(1+\sigma dW\right), \end{aligned} \tag{26}$$

When the EulerMaruyama method was applied with dr as Δr, the following backward differential equation was obtained:

$$S^*(r_j, t) = S^*(r_{j-1}, t) + \frac{\partial S}{\partial r}(r_{j-1}, t)\Delta r.\left[1 + \sigma\left(W(r_j) - W(r_{j-1})\right)\right] \tag{27}$$

The relationship between W_j and W_{j-1} could be expressed as follows (Higham, 2001):

$$\begin{aligned} W_j &= W_{j-1} + dW_j \\ &= W_{j-1} + \sqrt{\Delta r} N(0, r) \end{aligned} \tag{28}$$

where $N(m, \Sigma)$ is a normal random number with mean m and variance Σ. The properties and applications of Eq. (22), as solved by this method, are discussed in the following section.

5.1 Nature of proposed stochastic differential equation

Figure 9 shows the solution of the proposed stochastic differential equation when $\sigma = 0$ and 100. When $\sigma = 0$, the random term W is not included in the equation, such that it is identical to solving Eq. (20). Table 5 lists the input parameters of the exact solution. To set D, h, S_i, and S_t, the parameters of Tage tuff

Table 5. Input parameters of the proposed stochastic differential equation.

Initial Saturation degree S_i	Terminal saturation degree S_t	D (m^2/s)	h (m^{-1})	L (m)	Number of Fourier Series terms n	N
0.81	0	4.02×10^{-8}	12.2	1.0	100	300

determined in the previous section were used. The values of L and N were set to 1 m and 300, respectively. Figure 9 shows the results at different times, i.e., $t = 0$, 50, 100, and 1,000 d. Even if the random term σ was large, the exact solution reached a constant value, S_t, as t elapsed. For the difference in σ, solutions containing random terms with $\sigma = 20$ were distributed along the exact solution of Eq. (20) with $\sigma = 0$. As z increased, there was an increase in the uncertainty of the Brownian motion, such that there was increase in the influence of the random term. Brownian motion according to coordinate r was generated by the same normal random number with a mean of 0 and variance of r because the nature of the EDZ was assumed to be invariant with respect to time. Therefore, a relatively similar noise was generated

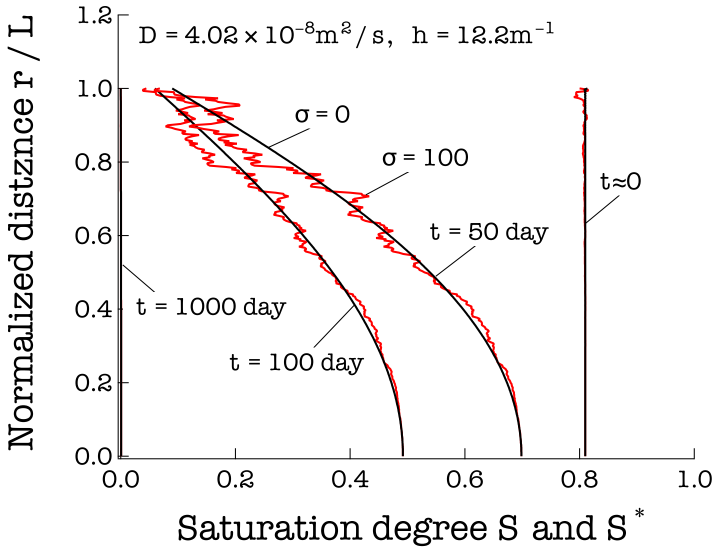

Figure 9. Saturation degree distributions of distance r due to volatility σ and time t for the EDZ and its characteristics.

in the results at the same r. Thus, this is a saturation distribution that reflects the properties of the EDZ.

Figure 10 was fixed at $t = 100$ d and $\sigma = 100$; the effect of N was investigated using the same parameter settings as those in Fig. 9. When N is exceedingly small, the difference step is large, such that the effect of the random term is excessively large. In the example in Fig. 10 ($N = 50$), S is ≥ 1, which is unrealistic. Additionally, when N is too small, and the effect of the random term is negligible. As the value of N also affects the uncertainty, a realistic value must be set. With this parameter setting, $N > 100$ would be preferable.

As described above, the proposed stochastic differential equation can express the properties of the EDZ and the influence of the random term can be determined via σ and N.

5.2 Method verification

Previous studies examined the difference in the saturated hydraulic conductivity of approximately 1–10 m behind the tunnel wall by conducting a laboratory test using a boring core or in situ hydraulic conductivity test (Hou, 2003), (Marschall et al., 2006), (Kurikami et al., 2008). In these studies, the hydraulic conductivity varied by 10^4 to 10^{10} m/s at the maximum as it approached the well wall. Particularly, the sedimentary rock sites targeted in this study have a maximum variation of 10^4 m/s (Kurikami et al., 2008). In our study, we considered the case where the saturated hydraulic conductivity, k_s, of the intact Tage tuff was disturbed by tunnel excavation of the tunnel and it increased by 10^4 m/s. In the rock mass at this time, if the hydraulic conductivity of the intact part ($r = 0$) and disturbed part ($r = L$) are linearly interpolated, the intermediate average hydraulic conductivity, k_s, is 5.7×10^{-11} m/s. As shown in Fig. 11, the validity of the proposed method was evaluated by calculating the stochastic differential equation of Eq. (22) using the average hydraulic conductivity, with $\sigma = 20$, and comparing it with the results of the hydraulic conductivity of the intact and disturbed parts, with $\sigma = 0$. This compar-

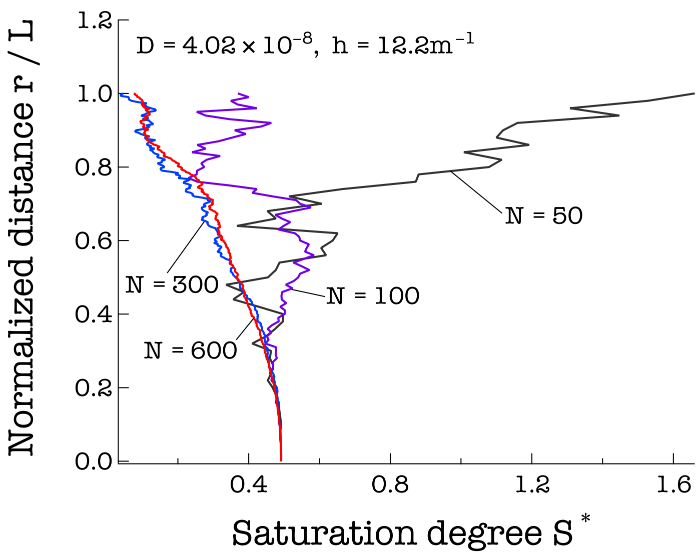

Figure 10. Effect of N on random terms in the saturation degree distribution of distance r

ative analysis used the data in Table 5, except for D. Each D was calculated using $k_s = 5.7 \times 10^{-11}$ m/s for the intact part and $k_s = 5.7 \times 10^{-7}$ for the disturbed part; $k_s = 5.7 \times 10^{-9}$ m/s was employed in the average case using the stochastic differential equation [Eq. (22)]. Equation (22) was solved 100 times with different Brownian motions, W. Figure 11 shows the results 10 d after the experiment, at which point the disturbed rock mass had already converged, where $S = 0.42$ at $r = L$. For stochastic differential equations, the average hydraulic conductivity lies between the results of the intact case and the disturbed case. Although the hydraulic conductivity was distributed in the actual bedrock, in the disturbed part near the tunnel wall, the hydraulic conductivity was small. Therefore, the behavior near the tunnel wall was similar to that of the disturbed case. As the saturation in the part with the high hydraulic conductivity near the mine wall decreases, there is also a decrease in the saturation in the intact part. Therefore, the saturation degree near $r = 0$ was considered smaller than that in the case for the intact hydraulic conductivity. Furthermore, considering that the hydraulic conductivity in the EDZ has a large variation, we can conclude that the results of the stochastic differential equation [Eq. (22)] are generally rational.

5.3 Random saturation distribution around a circular tunnel due to drying

Assuming that the drying phenomena occurs uniformly around the tunnel due to tunnel excavation without considering groundwater advection, we can estimate the saturation distribution around the tunnel using the 1-D stochastic differential equations proposed in this study. For example, this condition is applicable when constructing a deep tunnel, such as in geological disposal because it can be assumed that the head difference between the tunnel crown and invert is small from a macroscopic perspective. Considering the analysis area in Fig. 12, we assumed that the 1-D equation [Eq. (22)] can be applied in the r axis orientation in each circumferential direction, Θ. Figure 13 is a comparison of this analysis when $\sigma = 0$ and $\sigma = 30$. Here, using the Igor Pro graphing software, the 3-D coordinate points were contoured under exactly the same conditions. The set analysis conditions were the same as those in Table 5 by $N = 300$. These results represent 100 d after excavation.

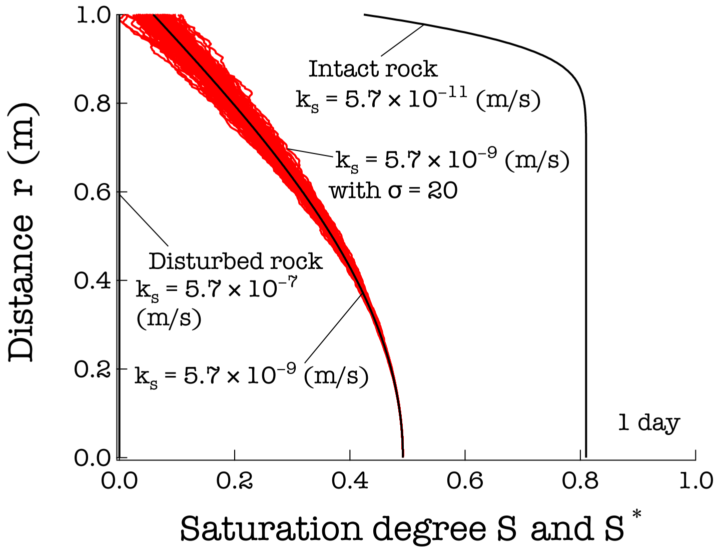

Figure 11. Comparison between the proposed stochastic differential equation using the average hydraulic conductivity and saturation distribution in the intact and disturbed parts.

As drying progressed from the wall surface of the tunnel, this part had the lowest saturation. The result of $\sigma = 0$ assumes that cracks do not occur during excavation; furthermore, a smooth curved surface with a saturation degree distribution can be confirmed. In contrast, for $\sigma = 30$, the variation in saturation became larger as it approached the tunnel wall surface. Moreover, for $\sigma = 30$, which considers the formation of the EDZ due to excavation, the variation in saturation increased as it approached the tunnel wall surface. This is not the same as the nature of the EDZ shown in Fig. 1.

Furthermore, in this analysis method, we can consider the anisotropy of the spatial variation in the saturation. The following function distributes σ in the circumferential direction, Θ:

$$\sigma = p|\sin\Theta| + q \tag{29}$$

where p and q are appropriate real numbers. Figure 14 shows the results of the same analysis performed at $p = 150$ and $q = 30$. This indicates that the variation in the saturation on the y axis is five-fold larger than that on the x axis. Sharp irregularities accumulate on the y axis (x axis), which is possible if the crustal pressure is anisotropic.

6 Conclusions

Evaluations of the water content in EDZs are indispensable for proper assessments of the deformation characteristics of the rock mass around a tunnel.

In this study, we derived a simple exact solution of Richards equation considering the Neumann boundary for drying deformation phenomena. Permeability test and mercury intrusion porosimetry tests were performed using Neogene tuff from Japan, and the water diffusion coefficient was specified based on the obtained parameters. The validity of the exact solution was confirmed using the specified water diffusion coefficient, which was compared with the change in the water content in the drying deformation test.

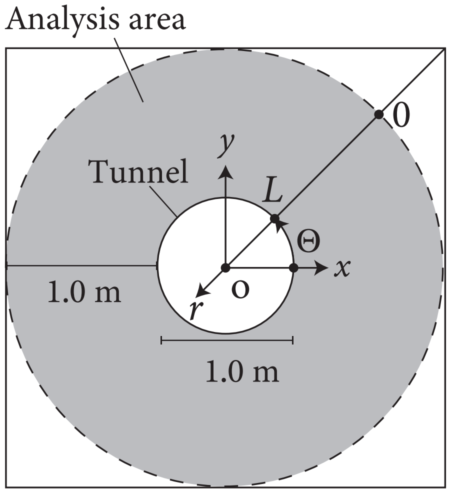

Figure 12. Analytical area of the EDZ. r is a coordinate system that radiates toward the center of the tunnel. $(x,\ y)$ is a two-dimensional Cartesian coordinate system. Θ is the angle between the x and r axes.

Furthermore, we proposed a new stochastic differential equation using the verified exact solution, which can express the change in the water content in an EDZ. In this equation, the hydraulic conductivity of the EDZ is expressed by indifferentiable Brownian motion. We confirmed the validity of the proposed stochastic differential equation based on calculations that assume a sedimentary rock tunnel to confirm that the properties of the water content in an EDZ can be appropriately expressed. Using the proposed 1-D stochastic differential equation, we showed that the water content distribution in the EDZ around a 2-D tunnel can also be evaluated.

Acknowledgments

This study was supported in part by a grant from the Ministry of Economy, Trade, and Industry, Japan.

References

ASTM. (2004). *Standard test method for determination of pore volume and pore volume distribution of soil and rock by mercury intrusion porosimetry (astm d4404-84).*

Autio, J., Siitari-Kauppi, M., Timonen, J., Hartikainen, K., & Hartikainen, J. (1998). Determination of the porosity, permeability and diffusivity of rock in the excavation-disturbed zone around full-scale deposition holes using the 14c-pmma and he-gas methods. *Journal of Contaminant Hydrology*, *35*(1-3), 19–29.

Barry, D., Parlange, J.-Y., Sander, G., & Sivaplan, M. (1993). A class of exact solutions for richards' equation. *Journal of Hydrology*, *142*(1-4), 29–46.

Broadbridge, P., Daly, E., & Goard, J. (2017). Exact solutions of the richards equation with nonlinear plant-root extraction. *Water Resources Research*, *53*(11), 9679–9691.

Esaki, T., Zhang, M., & Mitani, Y. (1996). Comparative tests for evaluating per-

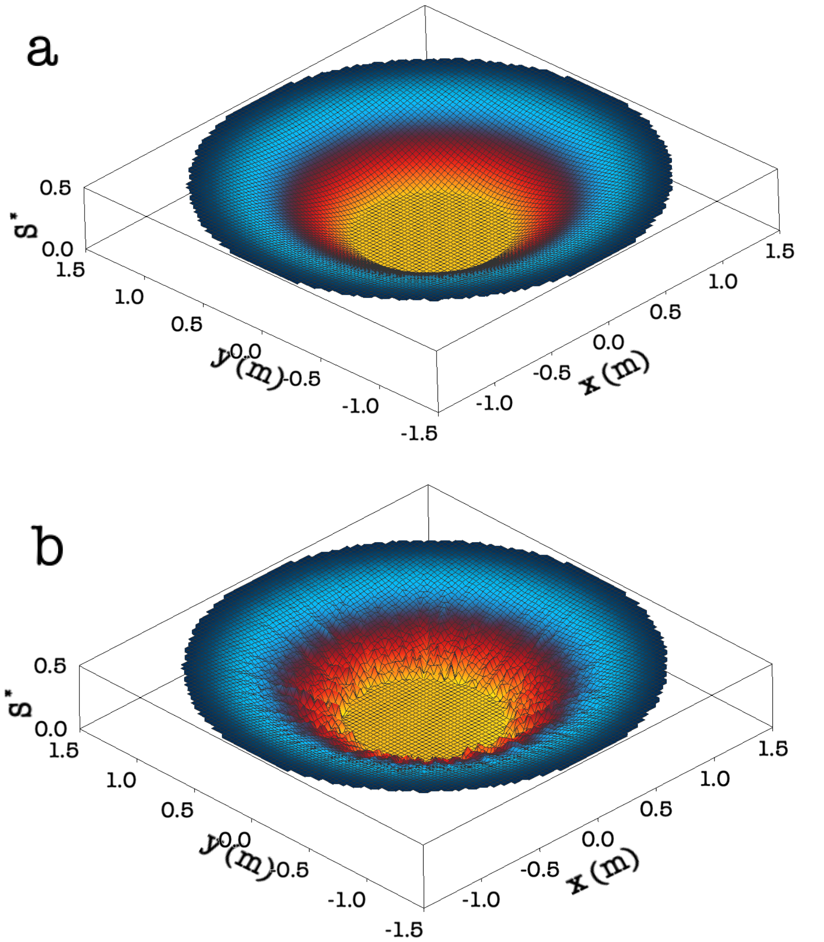

Figure 13. Comparison of the saturation degree distribution around the tunnel due to drying: (a) $\sigma = 0$ and (b) $\sigma = 30$.

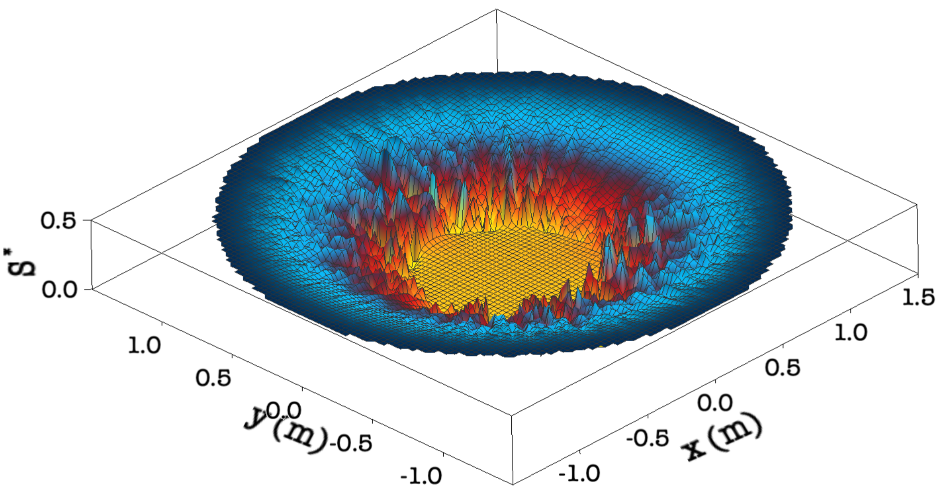

Figure 14. Analysis results for an anisotropic saturation degree distribution.

meability changes of a compacted bentonite/sand mixture during shear. *MRS Online Proceedings Library*, *465*, 979-986. doi: 10.1557/PROC-465-979

Farlow, S. (1993). *Partial differential equations for scientists and engineers.* Courier Corporation.

Farthing, M. W., & Ogden, F. L. (2017). Numerical solution of richards' equation: A review of advances and challenges. *Soil Science Society of America Journal*, *81*(6), 1257–1269.

Fleming, J. F., Parlange, J., & Hogarth, W. (1984). Scaling of flux and water content relations: comparison of optimal and exact results. *Soil Science*, *137*, 464-468.

Gardner, W. (1958). Some steady-state solutions of the unsaturated moisture flow equation with application to evaporation from a water table. *Soil science*, *85*(4), 228–232.

Higham, D. J. (2001). An algorithmic introduction to numerical simulation of stochastic differential equations. *SIAM review*, *43*(3), 525–546.

Hooshyar, M., & Wang, D. (2016). An analytical solution of richards' equation providing the physical basis of scs curve number method and its proportionality relationship. *Water Resources Research*, *52*(8), 6611–6620.

Hou, Z. (2003). Mechanical and hydraulic behavior of rock salt in the excavation disturbed zone around underground facilities. *International Journal of Rock Mechanics and Mining Sciences*, *40*(5), 725–738.

Kurikami, H., Takeuchi, R., & Yabuuchi, S. (2008). Scale effect and heterogeneity of hydraulic conductivity of sedimentary rocks at horonobe url site. *Physics and Chemistry of the Earth, Parts A/B/C*, *33*, S37–S44.

Lisjak, A., Tatone, B. S., Mahabadi, O. K., Grasselli, G., Marschall, P., Lanyon, G. W., ... Nussbaum, C. (2016). Hybrid finite-discrete element simulation of the edz formation and mechanical sealing process around a microtunnel in opalinus clay. *Rock Mechanics and Rock Engineering*, *49*(5), 1849–1873.

Marschall, P., Distinguin, M., Shao, H., Bossart, P., Enachescu, C., & Trick, T. (2006). Creation and evolution of damage zones around a microtunnel in a claystone formation of the swiss jura mountains. In *Spe international symposium and exhibition on formation damage control.*

Osada, M. (2014). Drying-induced deformation characteristics of rocks. In *Isrm international symposium-8th asian rock mechanics symposium.*

Richards, L. A. (1931). Capillary conduction of liquids through porous mediums. *Physics*, *1*(5), 318-333.

Ross, P., & Parlange, J.-Y. (1994). Comparing exact and numerical solutions of rochards' equation for one-dimentional infiltration and drainage. *Soil science*, *157*(6), 341–344.

Seiki, T. (2017). Introduction to oya tuff. *Journal of the Society of Materials Science, Japan*, *66*(11), 793-798. doi: 10.2472/jsms.66.793

Sun, W., & Cui, Y. (2020). Determining the soil-water retention curve using mercury intrusion porosimetry test in consideration of soil volume change. *Journal of Rock Mechanics and Geotechnical Engineering*, *12*(5), 1070-1079. doi: 10.1016/j.jrmge.2019.12.022

Thomas, L. K., Katz, D. L., & Tek, M. R. (1968). Threshold pressure phenomena in porous media. *Society of Petroleum Engineers Journal*, *8*(02), 174–184.

Togashi, Y., Imano, T., & Osada, M. (2021). Deformation characteristics of sedimentary rock due to continuous changes of moisture content in wetting process. In *Iop conference series: Earth and environmental science* (Vol. 703, p. 012021).

Togashi, Y., Imano, T., Osada, M., Hosoda, K., & Ogawa, K. (2021). Principal strain rotation of anisotropic tuff due to continuous water-content variation. *International Journal of Rock Mechanics and Mining Sciences*, *138*, 104646. doi: 10.1016/j.ijrmms.2021.104646

Togashi, Y., Kikumoto, M., Tani, K., Hosoda, K., & Ogawa, K. (2018). Detection of deformation anisotropy of tuff by a single triaxial test on a single specimen. *International Journal of Rock Mechanics and Mining Sciences*, *108*, 23–36. doi: 10.1016/j.ijrmms.2018.04.054

Togashi, Y., Kikumoto, M., Tani, K., Hosoda, K., & Ogawa, K. (2019). Non-axisymmetric and/or non-elementary response of anisotropic tuff in axisymmetric, elementary triaxial test. In *E3s web of conferences* (Vol. 92, p. 02008).

Togashi, Y., Kikumoto, M., Tani, K., Hosoda, K., & Ogawa, K. (2021). Determination of 12 orthotropic elastic constants for rocks. *International Journal of Rock Mechanics and Mining Sciences*, 104889. doi: (accepted)

Tracy, F. T. (2011). *Analytical and numerical solutions of richards' equation with discussions on relative hydraulic conductivity.* IntechOpen.

Watanabe, K., & Sato, K. (1979). Experimental study on permeability in fractured rock. *Proceedings of the Japanese conference on hydraulics*, *23*, 15-20. doi: 10.2208/prohe1975.23.15